Estimation of the Lyman-α line intensity in a lithium-based discharge-produced plasma source

Majid Masnavi, Mitsuo Nakajima, Eiki Hotta, and Kazuhiko Horioka
Department of Energy Sciences, Tokyo Institute of Technology, 4259 Nagatsuta, Midori-ku, Yokohama 226-8502, Japan

(Received 6 September 2007; accepted 27 October 2007; published online 7 January 2008)

Extreme ultraviolet (EUV) discharge-based lamps for EUV lithography need to generate extremely high power in the narrow spectrum band of 13.5 ± 0.135 nm. A simplified time-dependent collisional-radiative model and radiative transfer solution were utilized to investigate the wavelength-integrated Lyman-α line light outputs in a hydrogen-like lithium ion. The study reveals in particular that a steady-state or magnetically confined lithium plasma radiates in the desired spectrum band not less than 1 kW in 2π sr even at an ion density region as low as 10^{17} cm^{-3}.
 [DOI: 10.1063/1.2827477]

I. INTRODUCTION

Recent advances in the field of extreme ultraviolet (EUV) lithography[1–3] have revealed that laser-produced lithium (Li) and tin (Sn) plasmas or discharge-produced Sn plasma are source candidates for next-generation microelectronics.[4–6] In spite of impressive progress in the development of discharge EUV sources over the last several years,[7–10] only Sn plasma demonstrated large conversion efficiency (CE) of input power to emission in 2% bandwidth centered at the wavelength $\lambda = 13.5$ nm, the so-called in-band radiation. On the other hand, there are significant motivations for the interest in Li due to its pure spectrum and the lower energy ion generation in which it reduces debris problems significantly. In addition, considerably lower electron temperature (T_e) satisfies the condition to generate a required Li charge state that makes it possible to utilize various sources. Though there are many experimental results on Li, most of the previous works were performed in Z discharge-based plasmas,[7,11] in which the commonly observed low CE or in-band power is mainly due to the transient nature of such devices. In other words, for enhancing CE and output power of Li plasma, it is crucially important to prolong emission duration owing to its long radiative cooling time compared to Sn plasma.[12–14]

For high volume manufacturing, a high-repetition source having extremely high in-band power ($\simeq 180$ W) in the intermediate focus corresponding to $\simeq 1$ kW in 2π sr by a point-like plasma[3,10,15] is in demand. In this work, we are interested in estimating in-band power in nonlocal thermodynamic equilibrium (non-LTE) Li plasma. Thereby, we have calculated level populations and line intensities of various transitions by using a simplified zero-dimensional time-dependent collisional-radiative model (CRM) and some approximate solution methods of radiative transfer equations.

A computational model and assumptions are described briefly in Sec. II. The calculation results are presented and discussed in Sec. III for conditions relevant to EUV discharge plasma sources. This is followed by the conclusions.

II. CALCULATION MODEL AND ASSUMPTIONS

Figure 1 shows a schematic energy level diagram of Li charge states taken into account in our study. The CRM involves all of the electric dipole transitions in Li- and helium (He)-like ions based on the unresolved transition arrays (UTAs) framework of the Hebrew University Lawrence Livermore Atomic Code (HULLAC).[16,17] Since the output of the HULLAC is in a jj-coupling scheme, it is recognized as an LS-coupling scheme. For hydrogen (H)-like Li, calculation was carried out using the necessary atomic data of fine structure cited in the database of the National Institute of Standards and Technology.[18]

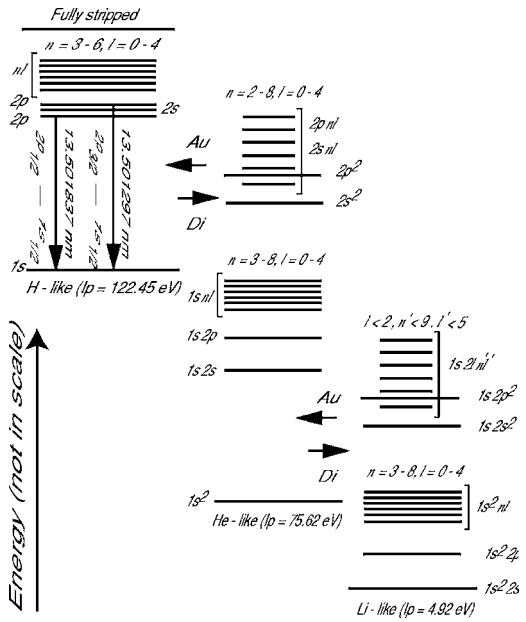

FIG. 1. Simplified energy level diagram of Li charge states taken into account in the calculation. The principal quantum number $n(n')$ and the orbital quantum number $l(l')$ for charge states including the autoionizing levels are shown. The ionization potentials (I_p) are taken from the HULLAC. The notations of Au and Di are, respectively, autoionization and dielectronic processes. The in-band emissions, namely the Lyman-α lines light outputs of $2p_{3/2}$-$1s_{1/2}$ (wavelength $\lambda = 13.501\ 297$ nm) and $2p_{1/2}$-$1s_{1/2}$ ($\lambda = 13.501\ 837$ nm) transitions in a H-like charge state, are calculated.

The CRM describing population distribution of atomic states can be written as

$$\frac{d}{dt}N_i = \sum_j M_{ji}N_j - \sum_j M_{ij}N_i + \Gamma, \tag{1}$$

in which N is the column vector of the energy level populations, M_{ij} (s^{-1}) is the rate describing a transition from state i to j, and Γ represents sources of the states. It is assumed that $\Gamma=0$. In CRM, all of the important atomic processes in discharge plasmas involving electron collisional ionization (γ), autoionization (Ω), electron collisional excitation (C) and deexcitation (D), spontaneous radiation (A), and recombination (Π) are included. Under the aforementioned assumption, Eq. (1) for the population density N_i^Z, i.e., the number density of level i of an ion of charge state Z, can be rewritten as

$$\begin{aligned}\frac{d}{dt}N_i^Z = &\underbrace{\left[\sum_j (n_e\gamma_{ji}^{Z-1,Z} + \Omega_{ji}^{Z-1,Z})\right]}_{S_{ij}^{Z-1}} N_j^{Z-1} + \underbrace{\left(n_e\sum_{i<i} C_{ji}\right)}_{X_{ij}^Z} N_j^Z \\ &- \underbrace{\left\{\left[\sum_{j<i} D_{ij} + \sum_{j>i} C_{ij} + \sum_{j>i} \gamma_{ij}^{Z,Z+1} + \sum_j \Pi_{ij}^{Z,Z-1}\right] n_e}_{R_{ij}^Z}\right. \\ &\left. + \sum_{j<i} \Omega_{ij}^{Z,Z+1} + \sum_{j<i} \psi(\tau_{ij})A_{ij}\right\} N_i^Z \\ &+ \underbrace{\left\{\sum_{j>i} [n_e D_{ji} + \psi(\tau_{ji})A_{ji}]\right\}}_{Y_{ij}^Z} N_j^Z + \underbrace{\left(n_e\sum_j \Pi_{ji}^{Z+1,Z}\right)}_{K_{ij}^{Z+1}} N_j^{Z+1},\end{aligned} \tag{2}$$

in which n_e is the electron density, τ is the optical depth in the spectral line center, and $\Pi=\alpha^t+\alpha^r+\alpha^d+\alpha^c/n_e$. Here, α^t, α^r, α^d, and α^c are, respectively, the three-body, radiative, dielectronic, and single electron capture charge-exchange recombination rate coefficients. The effect of opacity on level population is calculated by reducing the radiative decay rate by a factor equal to the escape factor (ψ). The summations include levels within the same charge state for C, D, and A, and among adjacent charge states for γ, Ω, and Π. The notation $j>i$ refers to levels j that have energies greater than that of level i. The subscripts ji refer to rates from level j to level i. The matrix M in Eqs. (1) and (2) using the notations of S, X, R, Y, and K is illustrated in Fig. 2. Equation (2) in a matrix form is easy to solve by a number of computer packages. Due to the nature of the problem, we used the MATLAB ODE suite of codes. Because Eq. (2) includes the opacity effect, the populations are calculated iteratively.[19] The electron density is determined self-consistently using the quasineutrality condition as $n_e=\bar{Z}\,n_i$. Here, $n_i=\Sigma\Sigma N_i^Z$ is the total ion density and $\bar{Z}$ is the average ionic charge state. Details of rate coefficients used in these calculations will be discussed elsewhere. In brief, we assumed that $\alpha^c=0$ and the

$$M = \begin{pmatrix}
-R_{1,j}^{0+} & Y_{1,j}^{0+} & . & Y_{1,m}^{0+} & K_{1,j}^{1+} & . & . & K_{1,n}^{1+} & 0 & 0 & 0 & 0 & 0 \\
X_{2,j}^{0+} & -R_{2,j}^{0+} & . & . & . & . & . & . & 0 & 0 & 0 & 0 & 0 \\
. & . & . & . & . & . & . & . & 0 & 0 & 0 & 0 & 0 \\
. & . & . & -R_{m,j}^{0+} & . & . & . & . & 0 & 0 & 0 & 0 & 0 \\
S_{\alpha,j}^{0+} & . & . & S_{\alpha,m}^{0+} & -R_{\alpha,j}^{1+} & Y_{\alpha,j}^{1+} & . & Y_{\alpha,n}^{1+} & K_{\alpha,j}^{2+} & . & . & K_{\alpha,l}^{2+} & 0 \\
. & . & . & . & . & . & . & . & . & . & . & . & 0 \\
. & . & . & . & . & . & . & . & . & . & . & . & 0 \\
S_{\beta,j}^{0+} & . & . & S_{\beta,m}^{0+} & X_{\beta,j}^{1+} & . & X_{\beta,n-1}^{1+} & -R_{\beta,j}^{1+} & . & . & . & . & 0 \\
0 & 0 & 0 & 0 & S_{\gamma,j}^{1+} & . & . & S_{\gamma,n}^{1+} & -R_{\gamma,j}^{2+} & Y_{\gamma,j}^{2+} & . & Y_{\gamma,l}^{2+} & K_{\gamma,l}^{3+} \\
0 & 0 & 0 & 0 & . & . & . & . & . & . & . & . & . \\
0 & 0 & 0 & 0 & . & . & . & . & . & . & . & . & . \\
0 & 0 & 0 & 0 & . & . & . & . & . & . & . & . & . \\
0 & 0 & 0 & 0 & 0 & 0 & 0 & 0 & S_{\eta,j}^{2+} & . & . & S_{\eta,l}^{2+} & -R_{\eta,l}^{3+}
\end{pmatrix}$$

FIG. 2. General form of the matrix M in Eq. (2) using the notations of S, X, R, Y, and K. It is assumed that the column vector of level populations is given by $N=[N_1^{0+}\ N_2^{0+}\ .\ .\ N_m^{0+}\ N_\alpha^{1+}\ .\ .\ N_\beta^{1+}\ N_\gamma^{2+}\ .\ .\ N_\delta^{2+}\ N_\eta^{3+}]^T$, in which T denotes the transpose of the vector. The N includes m Li-like (0^+) levels, n He-like (1^+) levels, and l H-like (2^+) levels as shown in M. Here, $\alpha=m+1$, $\beta=m+n$, $\gamma=m+n+1$, $\delta=m+n+l$, and $\eta=m+n+l+1$. In our calculation, $m=86$, $n=87$, and $l=34$. The appropriate zero elements in M correspond to atomic processes, in which they couple Z to a $Z+2$ charge state, such as double ionization or double charge-exchange recombination. Such processes are rare and hence are ignored. Please note that the M is the Jacobian of Eq. (2) and is usually sparse; it should be filled based on the density and temperature history. Equation (2) in a matrix form, namely $dN/dt=MN$, can be solved by using the MATLAB software even for a large number of atomic states.

Maxwellian energy distribution for plasma electrons. The rate coefficients are approximated by empirical formulas.[19–21] The excited states of adjacent charge states could be coupled to each other by ionization and recombination processes as shown in Fig. 2. However, Bernshtam *et al.* pointed out that[22] the difference between the empirical Lotz formula for the cross section of direct electron impact ionization among excited states of adjacent charge states compared to the distorted-wave calculation may become important for transient plasma with rapidly varying parameters. Please note that such an extremely transient condition is not relevant here. Nevertheless, based on these results and following Ref. 19, the ground and excited states having energies less than the ionization potential of stage Z are coupled to the ground state of ionization stage $Z+1$ by γ and vice versa the recombination processes of α^t and α^r. The autoionizing states of stage Z are coupled to levels that might be an excited state of ionization stage $Z+1$ by Ω, in which Ω was taken from the HULLAC, and the corresponding dielectronic captures are treated by using the detailed-balance relation.

III. RESULTS AND DISCUSSION

Under the LTE hypothesis, the radiation of thermal light sources is governed by the fundamental laws of thermodynamics. Their intensity and spectral distribution can be determined using Kirchhoff's law of absorption-emission and Planck's equation, respectively.[14] In general, the LTE assumption is not expected to be valid in the optically thin region relevant to discharge-based EUV sources. However, it allows us to calculate the maximum attainable or limiting

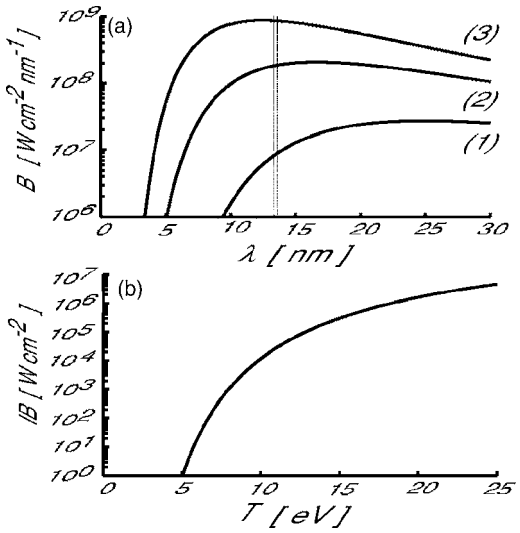

FIG. 3. (a) B vs λ: (1) $T=10$ eV, (2) 15 eV, and (3) 20 eV, respectively. The in-band region is shown as a reference. (b) In-band power IB of a single line at $\lambda=13.5$ nm, in which the line broadening is assumed to be due to the Doppler effect. This assumption gives the lower bound of the in-band power. The full width at half-maximum Doppler widths, for example, at $T=10$ and 15 eV, are, respectively, 1.34×10^{-3} and 1.64×10^{-3} nm, which are much narrower than the in-band region. (b) shows that a blackbody source having length=0.4 cm and radius 0.04 cm radiates the in-band power of 600 and 1.5×10^{4} W in 2π sr at $T=10$ and 15 eV, respectively.

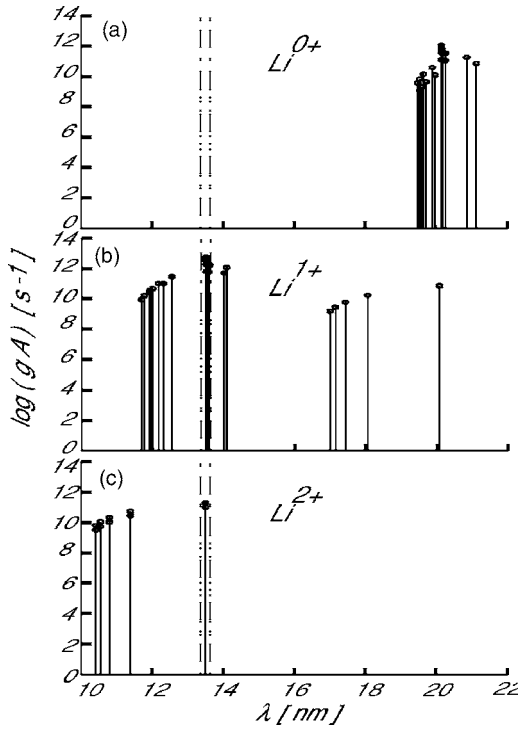

FIG. 4. The base 10 logarithm of g_jA_{ji} vs λ: (a) Li-like (Li^{0+}), (b) He-like (Li^{1+}), and (c) H-like (Li^{2+}) charge states. The Li- and He-like charge states are based on the UTA formalism of the HULLAC. The in-band region is shown as a reference. All of the transitions in (a) and the transitions having $\lambda<15$ nm in (b) originate from the autoionizing states. We ignored a possible contribution of the He-like ion to the in-band region. The line intensities are proportional to g_jA_{ji} values in sufficiently high density plasma, when the population of excited states approaches a Boltzmann distribution.

level of emission for a sufficiently opaque plasma. The spectral exitance B (W cm^{-2} nm^{-1}) of a black-body radiator versus wavelength λ is shown in Fig. 3(a) at different temperatures of $T=10$, 15, and 20 eV. Please note that Planck's equation (i.e., the line source function in the LTE situation) does not give information on the width of the spectral line. Thereby, to estimate the minimum in-band power IB (i.e., the power per unit area, integrated over the line profile in watt/square centimeter units), it is assumed that dominant line broadening is due to the Doppler effect using the ion temperature $T_i=T$. Figure 3(b) shows the in-band power of a blackbody radiator having a single line at $\lambda=13.5$ nm, integrated over the Doppler line profile versus T. This is the lower bound of the in-band power for the blackbody radiator due to the assumption of the Doppler profile. It is expected that, for example, the opacity broadening due to the transport of radiation through the plasma increases the linewidth.

The CRM is used to investigate the Lyman-α (hereafter Ly_α) emission in non-LTE Li plasma. Figure 4 shows the base 10 logarithm of g_jA_{ji} (the statistical weight g_j of upper state j times the radiative decay rate) modeled spectra of the Li charge states versus λ. As mentioned in Sec. II, the atomic structures of Li-, and He-like charge states are based on the UTA formalism.[16] Thus, the line positions in Figs. 4(a) and 4(b) represent the mean wavelengths of UTA. Since the configuration energy widths of the UTA are much smaller than the thermal energy, it is expected that it gives us an accurate results of $\bar{Z}$, at least in the density region discussed here.[23] Please note that all of the transitions in Fig. 4(a) and the transitions having $\lambda<15$ nm in Fig. 4(b) originate from the autoionizing states. Although the well-known satellite lines originating from transitions in a He-like ion (e.g., $2pnl$-$1snl$, particularly of those with $n\geq3$) may overlap with a H-like Ly_α line,[21] we ignored such a contribution of a He-like ion in calculation of the in-band power.

To investigate the ionization balance of Li charge states versus n_i and T_e, the time-dependent CRM is used. Since the electron-ion collision time is short in the density-temperature region discussed here, it is assumed that $T_i=T_e$. Figure 5(a) shows a typical calculation of fractional abundance f and $\bar{Z}$ versus time t. The initial level population N is calculated at equilibrium condition for $T_e=0.1$ eV and $n_i=10^{18}$ cm^{-3}. Then, it is assumed that T_e jumps to 12 eV, instantaneously, at constant n_i. The time evolution of n_e is proportional to $\bar{Z}$. The ion fractional abundances practically achieve equilibrium at $\simeq1$ μs, as can be seen in Fig. 5(a). That means if the plasma suffers a fast heating process such as shock wave heating, the ionization state distributions and consequently $\bar{Z}$ do not correspond to T_e until that time. Both lag behind T_e due to the relaxation effect of different ionization states, in particular in the low density regime relevant to discharge EUV sources. Note that the population of each charge state is $f\times n_i$. The ionization potential lowering is not addressed in the present calculation due to its negligible effect within our temperature and density range, in particular for He- and H-like charge states. Using the same calculation method described for Fig. 5(a), the ionization balance and $\bar{Z}$ vs T_e at different $n_i=10^{17}$ and 10^{18} cm^{-3} are estimated as shown in Figs. 5(b) and 5(c), respectively. Figures 5(b) and 5(c) indi-

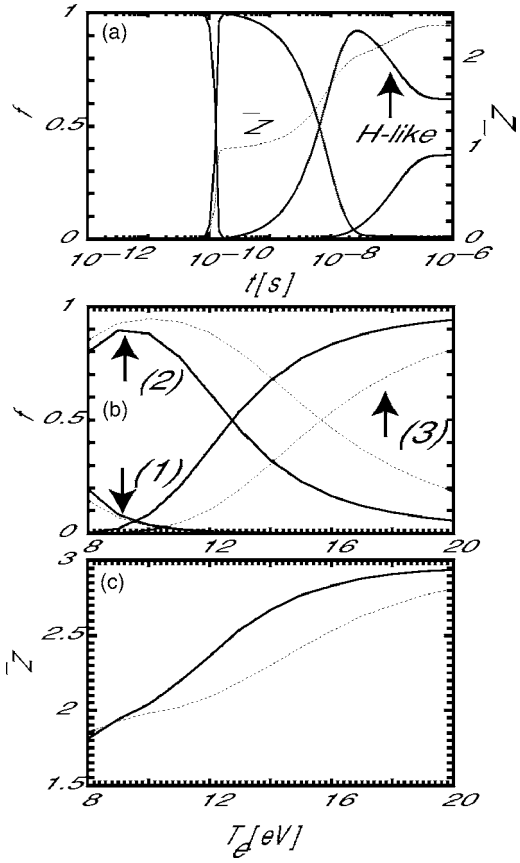

FIG. 5. (a) Time evolution of Li ion fraction f (solid lines: left ordinate) and $\bar{Z}$ (dashed line: right ordinate). The initial column vector of level populations is calculated at equilibrium condition for T_e=0.1 eV and n_i =10^{18} cm^{-3}. The initial $\bar{Z}$ is $\simeq 10^{-7}$. It is assumed that T_e jumps to 12 eV, instantaneously, at constant n_i. The ion fractions reach equilibrium at $\simeq 1$ μs. (b) Ion fractions of Li at equilibrium vs T_e. (1) He-like, (2) H-like, and (3) fully stripped charge states. The dashed and solid lines represent the calculation results at n_i=10^{17} and 10^{18} cm^{-3}, respectively. The ion fractions at given T_e are calculated by the same method as illustrated in (a). (c) The $\bar{Z}$ corresponding to (b) vs T_e, namely at equilibrium condition.

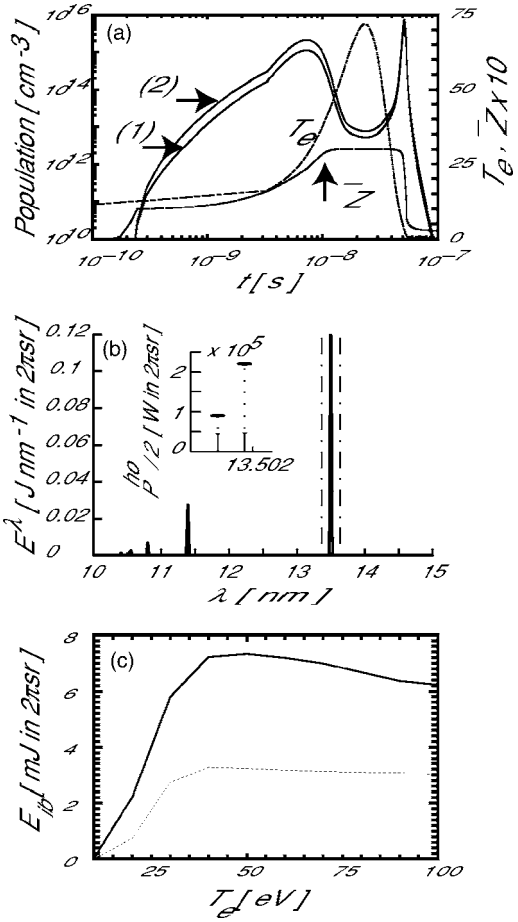

FIG. 6. (a) Time evolution of (1) $2p_{1/2}$ and (2) $2p_{3/2}$ level populations of the H-like stage (solid lines: left ordinate). A Gaussian-like profile is assumed for $T_e(t)$ (dot-dashed line: right ordinate), in which after a few nanoseconds it sharply increases to a maximum value of $\simeq$72 eV. It is assumed that $T_e(t=0)$=0.5 eV and $T_e(t \gtrsim 55)$ ns=0.5 eV. The last is assumed to calculate the recombination phase of a H-like ion. The calculation is carried out at constant n_i=10^{18} cm^{-3}. The $\bar{Z}$ (dashed line: right ordinate) is also shown where it is multiplied by a factor of 10 for a better view. (b) The half-calculated time-integrated radiated energy E^{λ} based on (a) vs λ over the region 10–15 nm. The spectrum is convoluted with a Gaussian profile of 0.02 nm FWHM. The total in-band energy is $\simeq$3.3 mJ in 2π sr. Inside of (b), the half-value of the instantaneous in-band power ($P^{h\nu}$/2) of Ly$_\alpha$ lines radiated at $t \simeq 7$ ns (solid lines: in ionization phase) and 50 ns (dotted lines: in recombination phase) is shown as a stem plot. A cylindrical plasma having a radius of 0.04 cm and a length of 0.4 cm is assumed. (c) The total in-band energy E_{ib} vs T_e at n_i=5×10^{17} (dotted line) and 5×10^{18} cm^{-3} (solid line). The E_{ib} at given T_e is calculated by the same method as illustrated in (a) and (b). The time history of T_e is kept constant, however its maximum value is changed. The calculation is carried out until 100 ns.

cate that the equilibrium value of H-like ion fractional abundance becomes maximized at $T_e \simeq 10$ eV. This is in agreement with the results of CRM using a steady-state assumption as described in Ref. 24, in particular in the low density region.

In pinch-type EUV sources, a high-energy-density plasma is formed by an electromagnetic implosion accompanied by a shock wave. At the final phase of implosion, the plasma temperature increases rapidly due to the thermalization of kinetic energy that is considered as a dominant heating process, under a condition of almost constant total ion density. The electrons are heated by hot ions to the required temperatures, and subsequently the plasma decays due to the hydrodynamic expansion. Thereby, it is clear that a realistic modeling of time-integrated in-band radiated energy would, in principle, require at least information about ionization dynamics of Li plasma and the plasma temperature-density history. These calculations can be carried out, but they shift the focus of the investigation to fluid dynamics and a given pulsed-power driver.[25] Because we are interested primarily in the kinetics behavior of Li plasma, we focus our efforts within the framework of zero-dimensional CRM. We now present some calculations that might be considered as a first approximation on the value of the in-band emission in transient EUV Li sources. Although the equilibrium value of the H-like stage becomes maximized at $T_e \simeq 10$ eV, in the transient case it might be observed at much higher T_e.[26]

Figure 6(a) shows the temporal dynamics of $2p_{1/2}$ and $2p_{3/2}$ level populations of the H-like stage in a transient case. A Gaussian-like temperature profile is assumed for the electrons at a constant n_i=10^{18} cm^{-3}. The dot-dashed curve in the figure shows the temperature profile used with the temperature scale on the right of the figure. Its full width at half-maximum (FWHM) is assumed to be $\simeq$20 ns, which

corresponds approximately to the time-scale characteristic of the Bennett equilibrium, i.e., the mean Alfvén transit time.[27] Please note that in some pinch-type EUV sources, the FWHM of T_e could be longer than this time due to the experimental conditions; see, for example, Ref. 11. The $\bar{Z}$ is also shown in Fig. 6(a), where it is multiplied by a factor of 10 for a better view. The time-integrated radiated energy for the emission between the upper state ϵ and the lower state ε is $E_{\epsilon\varepsilon}$ (Joule in 4π sr) $=\int P_{\epsilon\varepsilon}^{ho}(t)dt$, in which the instantaneous power for the emission line could be determined using a well-known formula as $P_{\epsilon\varepsilon}^{ho}$ (watt in 4π sr) $=N_{\epsilon}(t)\psi(t)A_{\epsilon\varepsilon}hcV/\lambda_{\epsilon\varepsilon}$.[21] Here, h is Planck's constant, c is the light speed, and V is the volume of plasma. The notation ho in $P_{\epsilon\varepsilon}^{ho}$ means the first formula that we used to estimate radiated power in the present calculation. The half-calculated time-integrated radiated energy based on Fig. 6(a) after a convolution by a Gaussian profile of 0.02 nm FWHM, namely E^{λ} (J nm^{-1} in 2π sr), is shown in Fig. 6(b) versus λ over the range 10–15 nm. We calculated the P^{ho} and E using an escape probability factor for a pure Doppler profile line. For cylindrical geometry, values of the Doppler profile escape factor have been calculated by Bhatia and Kastner,[28] and expressed for convenience as the logistic function $\psi \simeq \alpha_1/\{1+\exp[\alpha_2(\log \tau_D-\alpha_3)]\}$, where for the normal to cylindrical axis $\alpha_1=1.001\ 079\ 6$, $\alpha_2=2.321\ 213\ 6$, and $\alpha_3=0.223\ 355\ 45$. Here, τ_D is the optical depth in the center of the Doppler profile. The effect of opacity among excited states is also calculated. To estimate the opacity effect, it is assumed that the photon path length or plasma radius $R=0.04$ cm is constant. According to the étendue limit (≤ 3.3 mm^2 sr),[29] the plasma length is assumed to be 0.4 cm. The assumption of a pure Doppler profile line might be a good approximation in the low density regime relevant to discharge EUV sources because, for example, the FWHM Stark widths of Ly_{α} lines within the framework of Griem's semiempirical approach[30] are approximated to be 4.5×10^{-4} nm at $n_e=10^{19}$ cm^{-3} and $T_e=10$ eV, whereas the FWHM Doppler widths are 1.3×10^{-3} nm. Inside of Fig. 6(b), half of the instantaneous in-band power P^{ho} of Ly_{α} lines radiated at $t\simeq7$ and 50 ns is shown versus λ. The in-band radiated energy E_{ib} vs T_e at $n_i=5\times10^{17}$ and 5×10^{18} cm^{-3} is shown in Fig. 6(c). The E_{ib} at given T_e is calculated by the same method as described in Figs. 6(a) and 6(b). The time history of T_e is kept constant, however its maximum value is changed. Figure 6(c) shows that for $T_e \gtrsim 50$ eV, the E_{ib} reduces mainly due to the shorter ionization time of the H-like stage. Figures 6(b) and 6(c) reveal that although the instantaneous in-band power in ionization and recombination phases is high ($\simeq10^5$ W in 2π sr), the total in-band radiated energy for short-lasting Li plasma is very low. This conclusion is qualitatively in agreement with the experimental measurements in short-lasting Li plasma; see, for example, Ref. 7. Please note that in general, a typical discharge transient non-LTE plasma source presents strong temperature and density gradients. Thereby, the assumption of perfect homogeneity of the plasma is somewhat questionable. However, we think that this fact does not change our conclusion.

As stated in Sec. I, line emission is calculated based on two approximate solution methods of the radiative transfer equation. The first formula used here, which we call P^{ho}, is described in the last paragraph, in which it is expected to have a small error, at least for a strong spectral line.[21] The second solution is based on the integrated spectral exitance on the line profile emerging in a normal direction from a slab medium with an assumed spatially constant source function, which we call P^{cg}. The P^{cg}(W cm^{-2}) between two levels can be written as $P^{cg}=\pi\Xi W$, in which Ξ is the non-LTE source function and W is the equivalent linewidth.[14,21,26] In this formula, the total broadening of spectral lines will be affected by a combination of opacity effects and broadening mechanisms inherent to plasma (e.g., Stark and Doppler). We ignored natural line broadening, which becomes important only at extremely low temperature and density region. Note that opacity effects include modifications to line intensities as well as to linewidths. Here, a pure Doppler profile line is assumed. Thereby, the W can be written as $W=\Delta\lambda_D F$, in which $\Delta\lambda_D$ is the FWHM of the Doppler profile line and F is a dimensionless function of the τ_D.[31,32] Please note that F is equal to the line-center intensity factor multiplied by a corresponding half-width as defined in Ref. 32.

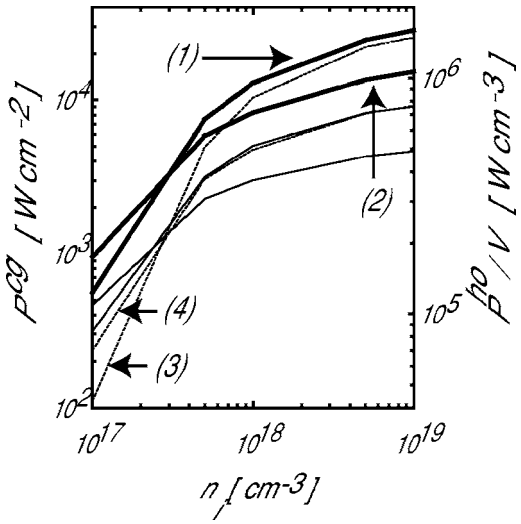

FIG. 7. The radiated power resulting from the $2p_{1/2}$-$1s_{1/2}$ and $2p_{3/2}$-$1s_{1/2}$ line transitions vs n_i for constant $T_e=10$ eV at steady-state condition, in which they are calculated based on two approximate solution methods of the radiative transfer equation. To estimate the opacity effect, it is assumed that the plasma radius $R=0.04$. The steady-state level populations are calculated using the same method as illustrated in Fig. 5(a). The bold solid lines are as follows: the P^{cg} calculated on transitions (1) $2p_{1/2}$ and (2) $2p_{3/2}$ to the ground state with the scale on the left of the figure. The dotted lines: (3) and (4) are, respectively, the P^{ho}/V calculated on the aforementioned transitions with the scale on the right of the figure. The light solid lines in the figure correspond to the bold lines of (1) and (2), in which they are calculated using the assumption of $F=1$.

Radiated powers resulting from the $2p_{1/2}$-$1s_{1/2}$ and $2p_{3/2}$-$1s_{1/2}$ line transitions versus n_i at constant $T_e=10$ eV, in which they are calculated using both approximations, are shown in Fig. 7. The steady-state level populations are calculated using the same method as illustrated in Fig. 5(a). The bold solid lines in Fig. 7 are as follows: the P^{cg} calculated on transitions (1) $2p_{1/2}$ and (2) $2p_{3/2}$ to the ground state with the scale on the left of the figure. The dotted lines, namely (3) and (4), are, respectively, the P^{ho} per plasma volume V cal-

culated on the aforementioned transitions with the scale on the right of the figure. A comparison among powers on different transitions reveals that the calculation results based on the P^{ho} and P^{cg} are approximately in agreement for a given plasma dimension, however the P^{ho} somewhat overestimates compared to the P^{cg}. The light solid lines in Fig. 7 correspond to the bold lines of (1) and (2), in which they are calculated using the assumption of $F=1$. Although this is not a mathematically correct assumption in the framework of the formula for P^{cg}, it allows us to compare non-LTE and LTE source functions. Note that the $\tau_D \gtrsim 2$ gives $F \gtrsim 1$. The Ly_α lines become optically thick quite easily, for example $\tau_D \gtrsim 6$ at $n_i=10^{17}$ cm^{-3}, $T_e=10$ eV, and $R=0.04$ cm. A comparison between the light solid lines in Fig. 7 and Figs. 3(b) at $T=10$ eV shows that the non-LTE source function in our calculation is less than the LTE case, namely in the case of a blackbody radiator, even at $n_i=10^{19}$ cm^{-3}. Note that for $n_e \gtrsim 5\times10^{18}$ cm^{-3}, the Voigt parameter $a=\sqrt{\ln 2}(\Delta\lambda_L/\Delta\lambda_D) \gtrsim 0.14$. Here, $\Delta\lambda_L$ is the FWHM of the Lorentz profile line. In such a situation and in homogeneous plasma in which self-reversal does not develop, a higher power is expected compared to values as shown in Fig. 7, due to the enhancement of W and the escape factor.[26,32,33] Nevertheless, we are interested primarily in the lower density region.

The total in-band power in 2π sr per plasma length (L) resulting from the $2p_{1/2}$-$1s_{1/2}$ and $2p_{3/2}$-$1s_{1/2}$ line transitions versus T_e and n_i is shown in Figs. 8(a) and 8(b), respectively. It is assumed that the plasma radius is $R=0.04$ cm. Note that the P^{cg} (W cm^{-2}) and P^{ho}/V (W cm^{-3}) are in different units, that is, the first one depends on the plasma area and the second on the plasma volume, as shown in Fig. 7. Thereby to make the same units, we define $P^c/L=P^{cg}\times 2\pi R$ and $P^h/L=P^{ho}\times \pi R^2/V$. The P^c/L and P^h/L are in watts in 4π sr per centimeter units. Therefore, the P_1 (W cm^{-1} in 2π sr) $=P^c/2L$ and P_2 (W cm^{-1} in 2π sr)$=P^h/2L$ in Fig. 8 should be multiplied by L (cm) to obtain total in-band power radiated in 2π sr at a constant R. The dotted and solid lines in Fig. 8(a) show the calculated value for P_1 and P_2 vs T_e at $n_i=5\times10^{17}$ and 5×10^{18} cm^{-3}. The dotted and solid lines in Fig. 8(b) show the calculated value for P_1 and P_2 vs n_i at $T_e=11$ and 15 eV. To find out the population distribution at steady-state condition, the same calculation method as discussed for Fig. 5(a) is carried out. Figure 8 reveals that at high density, the results of P_1 and P_2 are almost the same. In the high density and temperature region, the in-band power of Li plasma is high, as can be seen in Fig. 8(a). For example, the solid line (2) in Fig. 8(a) shows the total in-band power $P_1\times L\simeq 80$ kW in 2π sr for $n_i=5\times10^{18}$ cm^{-3}, $T_e=20$ eV, and $L=0.4$ cm. Imaging a long-lived plasma is possible, that is, radiation time $t_r\simeq 5$ μs. In such a situation, the Li plasma can radiate in-band power $P_1\times L\times t_r\times \nu \simeq 1200$ W in 2π sr using a $\nu=3$ kHz repetition-rate pulsed-power driver. One possible method to make such a high density, temperature, and long-lived plasma might be the hypocycloidal pinch apparatus.[34] However, the unique characteristics of such a device should be investigated and verified. An inspection of Figs. 8(a) and 8(b) reveals that a steady-state or magnetically confined Li plasma could also be an efficient EUV source even in the low density region.

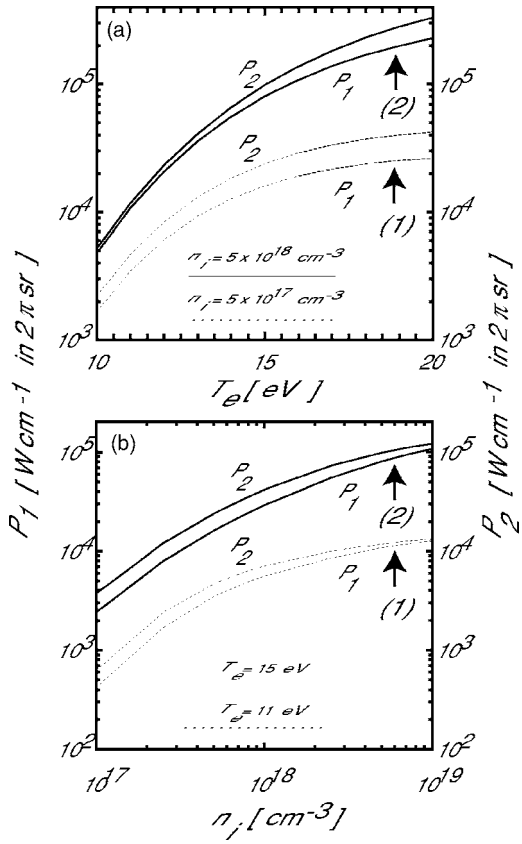

FIG. 8. The total in-band power in 2π sr per plasma length (L) resulting from the $2p_{1/2}$-$1s_{1/2}$ and $2p_{3/2}$-$1s_{1/2}$ line transitions: (a) vs T_e and (b) vs n_i. Here, it is assumed that $R=0.04$ cm. The steady-state level populations are calculated using the same method as illustrated in Fig. 5(a). The dotted line (1) and solid line (2) in (a) are calculated using the P_1 (left ordinate) at $n_i=5\times10^{17}$ and 5×10^{18} cm^{-3}, respectively. Two other lines, namely the dotted and solid lines, correspond to the power estimated using the P_2 (right ordinate) at $n_i=5\times10^{17}$ and 5×10^{18} cm^{-3}, respectively. The lines in (b) have the same definition, however they are calculated at $T_e=11$ and 15 eV, respectively. The P_1 and P_2 are, respectively, calculated using P^{cg} and P^{ho}. Please note that the value of P_1 and P_2 should be multiplied by the plasma length L (cm) to obtain total in-band power radiated in 2π sr at a constant R.

The dotted line (1) in Fig. 8(a) gives the $P_1\times L\simeq 10$ kW in 2π sr for $n_i=5\times10^{17}$ cm^{-3}, $T_e=20$ eV, and $L=0.4$ cm. Also, the solid line (2) in Fig. 8(b) shows the $P_1\times L \simeq 1$ kW in 2π sr for $n_i=10^{17}$ cm^{-3}, $T_e=15$ eV, and $L=0.4$ cm. Please note that the magnetic field in the region of $1\lesssim B\lesssim 4$ T is enough to trap such a plasma, namely, the mean beta value $\bar{\beta}=2\mu_0 kT_e n_i(1+\bar{Z})/B^2\simeq 1$ under assumption of $T_e=T_i$. Here, parameters have their usual meaning. Such a magnetic field could be generated by discharging a capacitor bank through a magnetic field coil or even by using permanent magnets. It should be noted here that we calculated and compared the power in the low density region to the available theoretical results of the Atomic Data and Analysis Structure (ADAS) and Los Alamos National Laboratory (LANL) suite of codes, as pointed out in Ref. 24. We found a good agreement among the results, although our calculation somewhat underestimates the power. A possible interesting venue where these results may be applied will be in confined plasma by magnetic fields in cusp-shaped configurations, or, in particular, in pinch-cusp devices.[35,36] Such investigation is in progress in our laboratory, but the details are

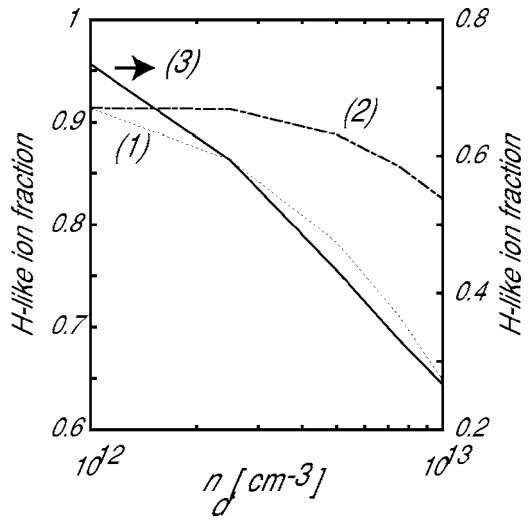

FIG. 9. Ion fractional abundance of H-like Li (Li^{2+}) vs donor ion density n_d, namely the density of the neutral Li beam. The relative velocity between the atom-ion undergoing charge exchange is assumed to be $v=10^7$ cm/s. Here, the constant ion density of $n_i=10^{17}$ cm^{-3} is assumed. The lines (1) and (2) are calculated at $T_e=10$ and 12 eV (left ordinate), respectively, and the solid line (3) at $T_e=8$ eV (right ordinate).

beyond the scope of the present study. To make such a plasma, it seems that plasma loss should be compensated by Li injection. Up to now, it was assumed that $\alpha^c=0$. The expected effect of charge-exchange recombination on ionization balance due to the injection of neutral Li might be estimated in the framework of the classical overbarrier model.[33,37,38] The cross section of charge transfer due to atom-ion collision can be written as $\sigma(\mathrm{cm}^2)\simeq 2.7\times 10^{-15}(2\sqrt{Z}+1)^2$. Here, it is assumed that the donor atom is neutral Li ($Ip=4.92$ eV) and Z is the charge of the acceptor ion. Thereby, the rate coefficient $\alpha^c\ (\mathrm{s}^{-1})=n_d v\sigma W_{nl}$, in which n_d is the donor atom density, v is the relative velocity of the atom-ion, and W_{nl} is the l-distribution probability factor as discussed in Ref. 38. Considering a Li plasma already formed, the effect of charge-exchange recombination on H-like ion abundance versus n_d due to the injection of a neutral Li beam having constant density is shown in Fig. 9. Here, it is assumed that $v=10^7$ cm/s, and single charge transfer among neutral Li and other charge states is calculated. Figure 9 reveals that although the effect of charge-exchange recombination is high, in particular in high n_d and v, our result seems to indicate that in such a situation a few higher electron temperature compared to Fig. 5(b) is enough to obtain approximately the same average ion charge state as well as the in-band power.

IV. CONCLUSIONS

Using a simplified time-dependent collisional-radiative model and two approximate solution methods of the radiative transfer equation for an isotropic Li plasma, we have calculated the Lyman-α lines in-band power versus ion density and electron temperature for conditions relevant to EUV discharge plasma sources. The calculation results show that the total in-band radiated energy for short-lasting transient Li plasma is very low, even at high density and electron temperature. Thereby, it is expected that the inherent conversion efficiency of Li plasma in such a situation also becomes low owing to its long radiative cooling time. Our results show that a long-lived Li plasma ($\simeq 5$ μs) in the high ion density ($\simeq 5\times 10^{18}$ cm^{-3}) and electron temperature ($\simeq 20$ eV) region has the potential to radiate in-band power not less than 1 kW in 2π sr by using a pulsed-power driver having a 3 kHz repetition rate. One possible method to make such a high density, temperature, and long-lived plasma might be the hypocycloidal pinch apparatus. The analysis shows in particular that a steady-state or magnetically confined Li plasma could also be an efficient EUV source even in the low density and temperature region. An in-band average power not less than 1 kW in 2π sr is expected in the ion density $n_i>10^{17}$ cm^{-3} and electron temperature $T_e>10$ eV region. A possible approach to make such a long-lasting Li plasma could be a combination of both pinch-cusp configurations.

ACKNOWLEDGMENTS

One of the authors (M.M.) gratefully acknowledges Akira Sasaki for making the data of the HULLAC code available, and also Tohru Kawamura and Tomonao Hosokai for valuable discussions. This work was sponsored in part by the New Energy and Industrial Technology Development Organization (NEDO) and the Extreme Ultraviolet Lithography System Development Association (EUVA) of Japan.

[1] D. Attwood, *Soft X-Rays and Extreme Ultraviolet Radiation* (Cambridge University Press, New York, 1999).
[2] *EUV Sources for Lithography*, edited by V. Bakshi (SPIE, Bellingham, WA, 2005).
[3] B. Wu and A. Kumar, J. Vac. Sci. Technol. B **25**, 1743 (2007).
[4] See several contributions in EUVL Symposium, November, 2005, San Diego. Available online: http://www.sematech.org; directory: meetings/archives/litho/euvl/7470/index.htm
[5] V. Sizyuk, A. Hassanein, and T. Sizyuk, J. Appl. Phys. **100**, 103106 (2006).
[6] V. Borisov, A. Eltzov, A. Ivanov, O. Khristoforov, Yu. Kirykhin, A. Vinokhodov, V. Vodchits, V. Mishhenko, and A. Prokofiev, Proc. SPIE **6611**, 66110B (2007).
[7] M. A. Klosner, H. A. Bender, W. T. Silfvast, and J. J. Rocca, Opt. Lett. **22**, 34 (1997).
[8] C. Jiang, A. Kuthi, M. A. Gundersen, and W. Hartmann, Appl. Phys. Lett. **87**, 131501 (2005).
[9] B. S. Bauer, V. Makhin, S. Fuelling, and I. R. Lindemuth, Proc. SPIE **6151**, 61513N (2006).
[10] J. Jonkers, Plasma Sources Sci. Technol. **15**, S8 (2006).
[11] W. N. Partlo, I. V. Fomenkov, I. R. Oliver, and D. L. Birx, Proc. SPIE **3997**, 136 (2000).
[12] M. Masnavi, M. Nakajima, A. Sasaki, E. Hotta, and K. Horioka, Appl. Phys. Lett. **89**, 031503 (2006).
[13] A. Nagano, T. Inoue, P. Nica, S. Amano, S. Miyamoto, and T. Mochizuki, Appl. Phys. Lett. **90**, 151502 (2007).
[14] M. Masnavi, M. Nakajima, E. Hotta, K. Horioka, G. Niimi, and A. Sasaki, J. Appl. Phys. **101**, 033306 (2007).
[15] U. Stamm, J. Kleinschmidt, D. Bolshukhin, J. Brudermann, G. Hergenhan, V. Korobotchko, B. Nikolaus, M. C. Schrmann, G. Schriever, C. Ziener, and V. M. Borisov, Proc. SPIE **6151**, 615100 (2006).
[16] M. Klapisch, A. Bar-Shalom, J. Oreg, and D. Colombant, Phys. Plasmas **8**, 1817 (2001).
[17] JAERI Atomic Database, available online: http://gadget.apr.jaeri.go.jp/atomic_data/work/Li.html
[18] NIST Atomic Spectra Database, available online: http://physics.nist.gov/cgibin/AtData/levels_form
[19] R. W. Lee and J. T. Larsen, J. Quant. Spectrosc. Radiat. Transf. **56**, 535 (1996).
[20] D. Duston and J. J. Duderstadt, J. Appl. Phys. **49**, 4388 (1978).

[21]D. Salzman, *Atomic Physics in Hot Plasmas* (Oxford University Press, New York, 1998).
[22]V. A. Bernshtam, Y. V. Ralchenko, and Y. Maron, J. Phys. B **33**, 5025 (2000).
[23]A. Bar-Shalom, J. Oreg, W. H. Goldstein, D. Shvarts, and A. Zigler, Phys. Rev. A **40**, 3183 (1989).
[24]S. D. Loch, C. J. Fontes, J. Colgan, M. S. Pindzola, C. P. Ballance, D. C. Griffin, M. G. O'Mullane, and H. P. Summers, Phys. Rev. E **69**, 066405 (2004).
[25]A. Hassanein, V. Sizyuk, V. Tolkach, V. Morozov, T. Sizyuk, B. J. Rice, and V. Bakshi, Proc. SPIE **5374**, 413 (2004).
[26]G. Schriever, K. Bergmann, and R. Lebert, J. Appl. Phys. **83**, 4566 (1998).
[27]M. A. Liberman, J. S. D. Groot, A. Toor, and R. B. Spielman, *Physics of High-Density Z-Pinch Plasmas* (Springer, New York, 1999).
[28]A. K. Bhatia and S. O. Kastner, J. Quant. Spectrosc. Radiat. Transf. **58**, 347 (1997).
[29]V. Banine and R. Moors, J. Phys. D **37**, 3207 (2004).
[30]H. R. Griem, Phys. Rev. **165**, 258 (1968).
[31]M. Masnavi, M. Nakajima, A. Sasaki, E. Hotta, and K. Horioka, Jpn. J. Appl. Phys., Part 1 **43**, 8285 (2004).
[32]S. O. Kastner and A. K. Bhatia, J. Quant. Spectrosc. Radiat. Transf. **58**, 217 (1997).
[33]T. Fujimoto, *Plasma Spectroscopy* (Clarendon, Oxford, 2004).
[34]J. H. Lee, D. R. McFarland, and F. Hohl, Phys. Fluids **20**, 313 (1977); J. H. Lee, D. R. McFarland, and F. Hohl, Appl. Opt. **19**, 3343 (1980).
[35]F. R. Scott and R. F. Wenzel, Phys. Rev. **119**, 1187 (1960).
[36]J.-P. H. Watteau, Phys. Fluids **4**, 607 (1961).
[37]R. K. Janev, Phys. Rev. A **28**, 1810 (1983).
[38]F. B. Rosmej, H. R. Griem, R. C. Elton, V. L. Jacobs, J. A. Cobble, A. Ya. Faenov, T. A. Pikuz, M. Geibel, D. H. H. Hoffmann, W. Sub, D. B. Uskov, V. P. Shevelko, and R. C. Mancini, Phys. Rev. E **66**, 056402 (2002).